HETEROGENEOUS INTEGRATION FOR HYBRID ACOUSTIC DEVICES: GAN/CU/YIG MAGNETOELASTIC HBARS

Vikrant J. Gokhale[1], Brian P. Downey[1], Pallavi Dhagat[2], Albrecht Jander[2], Shawn Mack[1], D. Scott Katzer[1], Jason A. Roussos[1], and David J. Meyer[1]
[1]US Naval Research Laboratory, Washington DC, USA
[2]Oregon State University, Corvallis, OR, USA

ABSTRACT

This work presents the heterogeneous integration of thin film acoustic devices using micro-transfer printing (MTP). Our approach enables the transfer of a high quality acoustic transducer grown epitaxially on a source substrate (6H-SiC), onto a target substrate that is not compatible with epitaxy [here, yttrium iron garnet (YIG)], with no degradation in measured RF/acoustic performance. The resulting integrated device is a magnetoelastic high overtone bulk acoustic resonator (ME-HBAR), which can hybridize acoustic and spin waves (phonons and magnons). We describe the MTP process, along with RF/acoustic and magnetoelastic characterization of the ME-HBAR.

INTRODUCTION

It is well known that the performance and capabilities of a microelectronic system can be enhanced by the heterogeneous integration of various optimized sub-components in the form of ‘chiplets’ onto a common target substrate. Depending on the application, the target substrate could simply be a cost-effective platform (CMOS wafer with readout routing), a flexible platform (rapid roll-to-roll assembly), or an efficient thermal spreader for power electronics (diamond). Alternately, one can choose a functional target substrate with physical characteristics that are crucial to the MTP device operation. In prior work, we have shown that epitaxial AlGaN/GaN high electron mobility transistors (HEMTs) can be individually transferred to an arbitrary target substrate using micro-transfer printing (MTP) [1], without significant change in performance. We add to this capability by demonstrating the MTP integration of epitaxially grown GaN-based piezoelectric RF-MEMS devices.

As a demonstration of this principle and capability, we take GaN-based epitaxial high overtone bulk acoustic resonators (epi-HBARs) grown on 6H-SiC, and transfer the piezoelectric transducers to a ferrimagnetic yttrium iron garnet ($Y_3Fe_5O_{12}$ or YIG) substrate, forming magnetoelastic HBARs (ME-HBARs). The transfer is mediated by an epitaxial NbN sacrificial layer, and a commercially available pick-and-place MTP tool and process that can be scaled to industrial manufacturing. The MTP process decouples the highly optimized Group III – Nitride epitaxy process from the functional YIG target substrate. To the best of our knowledge, this is the first demonstration of MTP integration of individual MEMS acoustic transducers.

The resulting YIG ME-HBARs can support low-loss propagation and confinement of both acoustic and spin waves simultaneously. Such hybrid phonon-magnon coupled devices can be used as sensors, magnetically tunable oscillators, filters, or parametric amplifiers, with applications for both classical and quantum signal processing systems [2-6]. While ME-HBARs have been fabricated by evaporating/sputtering metals and piezoelectric layers on to YIG and other ferroic substrates, the fabrication of such devices is constrained by nucleation dynamics, sputtered grain size/quality, axis optimization, and thermal budgets of the deposition process, all of which restrict the type and quality of potential material combinations [7, 8].

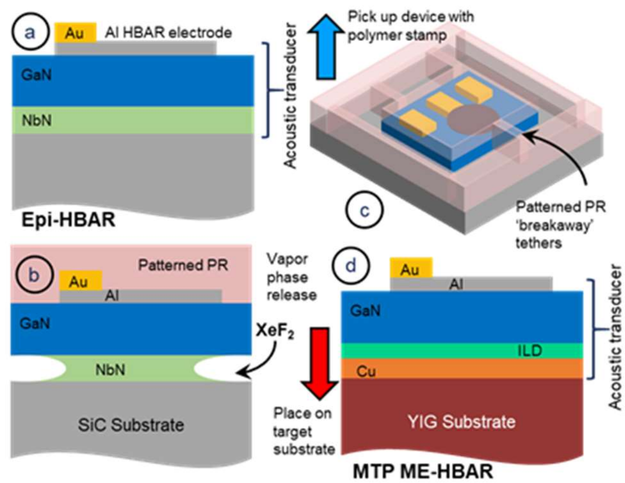

Figure 1: Micro-transfer printing (MTP) process flow to transfer a GaN-based piezoelectric acoustic transducer grown epitaxially on 6H-SiC, to a ferrimagnetic YIG substrate, forming a magnetoelastic GaN/Cu/YIG HBAR. Not to scale.

While HBARs made from YIG thin films have been demonstrated (with gadolinium gallium garnet as the substrate), the phonon-magnon interaction volume in such devices is restricted only to the YIG film [9, 10]. Unlike electronic or surface acoustic wave devices, the main physical phenomena in ME-HBARs (phonons and magnons) traverse the bonded interface, and thus can interact in the entire substrate.

FABRICATION PROCESS

Epitaxial transducer heterostructure

The design, development, and RF/acoustic characterization of epi-HBARs grown on SiC substrates using molecular beam epitaxy (MBE) has been described in previous work [11, 12]. The subsequent MTP process flow for the ME-HBAR is summarized in Fig. 1. First, an AlGaN/GaN/AlN/NbN heterostructure (thicknesses of 25 nm/1.2 µm/45 nm/50 nm respectively) is grown on a 370 µm thick 6H-SiC substrate). The *c*-axis oriented AlGaN/GaN/AlN piezoelectric layers are grown at temperatures up to 725 ˚C. The combination of heterostructure and epitaxial source substrate is carefully chosen to provide a) close lattice matching required for electronic-grade AlGaN/GaN, and b) the acoustic impedance matching required for efficient power transfer [13]. For the purposes of this experiment, the AlGaN barrier was etched using a Cl_2/BCl_3 plasma, removing the 2D electron gas at the AlGaN/GaN interface. The circular top electrode (Cr/Al, 10 nm/50 nm) is fabricated by electron beam evaporation, and liftoff. Thick Au contact pads (200 nm) are deposited and patterned next to the transducer to provide a coplanar waveguide (CPW) for RF input signals. ‘As-grown’ epi-HBARs are characterized to gauge their baseline RF/acoustic performance and properties. Next, a trench is etched around individual devices (Cl_2/BCl_3 plasma), isolating individual devices, and providing access to the underlying NbN sacrificial release layer.

978-1-940470-04-7/HH2022/$25©2022TRF
DOI 10.31438/trf.hh2022.9

Solid-State Sensors, Actuators, and Microsystems Workshop
Hilton Head Island, South Carolina, June 5-9, 2022

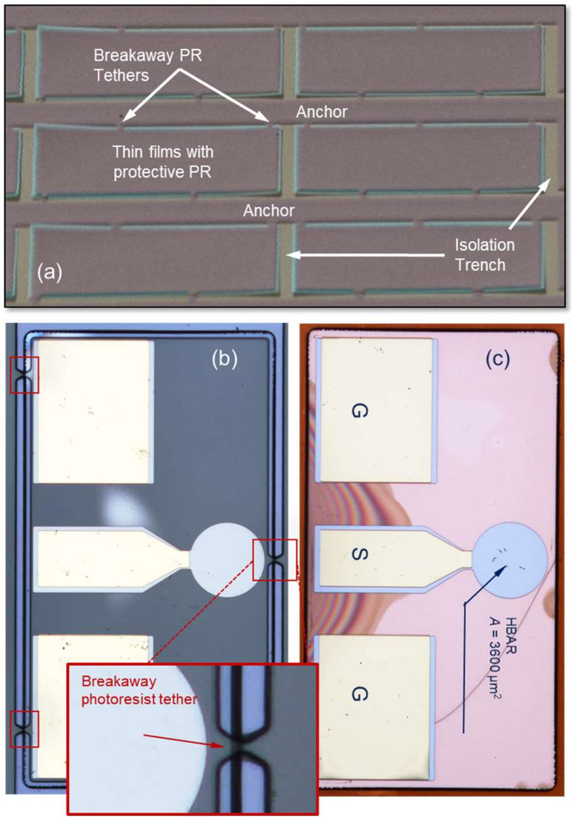

Figure 2. (a) False color electron microscope image of an array of released GaN chiplets before the MTP process. Optical microscope images of (b) released devices held in place with breakaway PR tethers (inset), and (c) transfer printed onto a Cu/YIG surface.

A photoresist (PR) layer is subsequently patterned to provide mechanical anchors on the SiC substrate and 'breakaway' tethers to hold the HBARs in place during the release etch, and to provide a protective layer on top of the HBARs during transfer (Fig. 2). The NbN layer is then selectively removed using XeF_2 vapor phase etching, releasing the GaN acoustic transducers [14], but leaving them suspended by the PR tethers (Fig. 2).

Micro Transfer Printing of individual transducers

Separately, a 100 nm thick Cu film is evaporated on to a 350 µm thick <111> YIG target substrate (MTI Corporation). YIG is a magnetostrictive and ferrimagnetic material well known for its low acoustic and spin wave damping. The Cu film has low acoustic mismatch with YIG, and replaces NbN as the bottom electrode in the transducer. A diluted Intervia 8023-10 interlayer dielectric (ILD) is spun onto the Cu/YIG target substrate forming an adhesion layer (measured to be 10 nm thick). An X-Celeprint MTP tool [15, 16] is used to transfer individual GaN acoustic transducers from the source substrate to specific locations on the Cu/YIG target substrate, forming an Al/GaN/AlN/Cu/YIG ME-HBAR. A UV flood exposure and bake cures the ILD, and O_2 plasma removes ILD from the open areas of the target substrate. Critically, unlike the 725 °C MBE step used to grow the heterostructure, a post-transfer hotplate bake at 185 °C is the highest process temperature step for the YIG target substrate. Optical microscope images of the post-transfer ME-HBAR (Fig. 2) show that while there is some curling due to stress, the transducer electrode is transferred into contact with the target substrate. Stress compensating films or patterns in the open areas of the chiplet can be explored in the future.

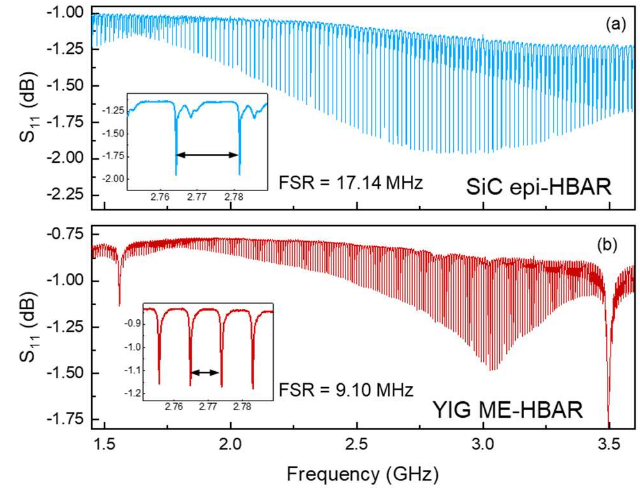

Figure 3. A comparison of the RF reflection spectra of the epi-HBAR and the ME-HBAR after successful transfer printing. Note the expected decrease in FSR associated with the slower acoustic velocity in the YIG substrate.

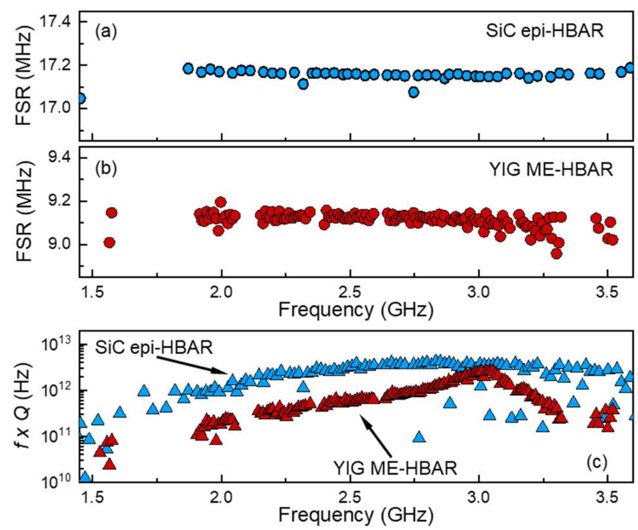

Figure 4. A comparison of the RF reflection spectra of (a) the epi-HBAR, and (b) the ME-HBAR after successful transfer printing. Note the expected decrease in FSR associated with the slower acoustic velocity in the YIG substrate. (c) Measured ($f \times Q$) products for both the epi-HBAR and the ME-HBAR show that there is no degradation in performance due to the MTP process.

DEVICE CHARACTERIZATION

Radio frequency / acoustic characterization

For any HBAR, important RF/acoustic parameters include the multi-mode RF spectral envelope, the spacing between overtones (the free spectral range or FSR), and the frequency-quality factor figure of merit ($f \times Q$) product for all m modes. We compare the epi-HBARs as grown on 6H-SiC with the corresponding ME-HBARs by characterizing their RF/acoustic performance.

All devices shown here are measured at room temperature using a vector network analyzer (VNA) and coplanar ground-signal-ground (GSG) probes. High resolution, sequential sweeps are acquired and the composite spectra are shown in Fig. 3. While there are changes in the shape of the RF reflection envelope, the RF reflection response (S_{11}) of the ME-HBAR is not significantly degraded when compared to that of the original epi-HBAR, indicating good transfer. The two strong but low-Q modes at 1.55 GHz and 3.50 GHz in the ME-HBAR spectrum (Fig. 3(b)) are believed to be unwanted surface cavity overtones trapped by the parallel edges of the chiplet. These modes can be easily eliminated by apodizing the chiplet or by the use of damping layers.

To a first order, the FSR for any HBAR can be approximated as $FSR = v/2t$, where v is the substrate acoustic velocity and t is the substrate thickness. A detailed study of the FSR, its dependence on the heterostructure, and its use as a diagnostic for impedance matching can be found in prior work [13]. Here, FSR values of 17.14 MHz (Fig. 3(a)) and 9.10 MHz (Fig. 3(b)) are experimentally observed for the epi-HBAR and ME-HBAR respectively. Based on the substrate thicknesses, we can extract acoustic velocities of 12,684 m/s for the epi-HBAR and 6370 for the ME-HBAR. Extracted values are close to values from the literature: 13,300 m/s for SiC and 6220 m/s for <111> YIG [2, 17]. The extracted $f \times Q$ products for both the epi-HBAR and the ME-HBAR show that there is no obvious degradation in performance for the MTP ME-HBAR relative to the original epi-HBAR (Fig. 4(c)). Further experiments are needed to investigate the performance of the best performing SiC based epi-HBARs ($f \times Q > 10^{15}$ Hz at room temperature) when transferred to YIG and other target substrates. Specifically, it would be useful to separate losses due to the transfer interface and the adhesion ILD film from the losses in the target substrate.

Magnetoelastic characterization

In order to characterize their magnetoelastic performance the MTP ME-HBARs are wire-bonded and mounted on a rotating stage within the gap of a laboratory electromagnet. The frequency response of the ME-HBARs is measured as a function of magnetic field, **B**. Two representative measured responses are shown in Fig. 4, for zero applied magnetic field, and for an applied magnetic field of B_x = 56 mT (in-plane component), and B_z = 180 mT (normal component). In a spectral region near 2.75 GHz (the 305th mechanical overtone mode of the ME-HBAR), coupling and hybridizing of the acoustic waves with corresponding spin wave modes at this magnetic bias is observed [18], leading to a shift in the resonant frequency of the acoustic modes. In a narrow part of this region near $m = 305$, the phonon-magnon coupling completely attenuates the mechanical mode. The dispersion of the phonon-magnon coupling can be verified by plotting the frequency of each mode 'm' against the corresponding wavenumber $1/\lambda = m/2t$. The effect of hybridizing into magnetoelastic waves is clearly visible as a deviation from the normally linear dispersion of acoustic waves around 2.75 GHz (Fig. 5). While the HBAR provides multiple phonon modes over a wide RF spectrum by design, an appropriate magnon mode can be selected by tuning the magnetic bias. Comprehensive experiments along with a detailed model of the multi-mode magnon-phonon hybridization shall be discussed in future work. The frequency shift of mode $m = 305$ is shown in Fig. 6 as a function of the in-plane and normal components of the magnetic field. The bright arc in the top right corner of Fig 6(a) corresponds to conditions where the spin wave and acoustic wave dispersion curves cross and form hybrid magneto-elastic waves with high damping. Sufficiently far from this crossover, the magnetization dynamics and associated damping can be neglected and the frequency shift attributed to the ΔE effect, a dependence of the elastic modulus on the magnetization state in magnetostrictive materials [19]. The ΔE effect is highlighted in Fig. 6(b), with an expanded color scale. A frequency tuning of up to 100 kHz (~1% of the FSR) can be achieved in this regime with no discernable effect on the damping.

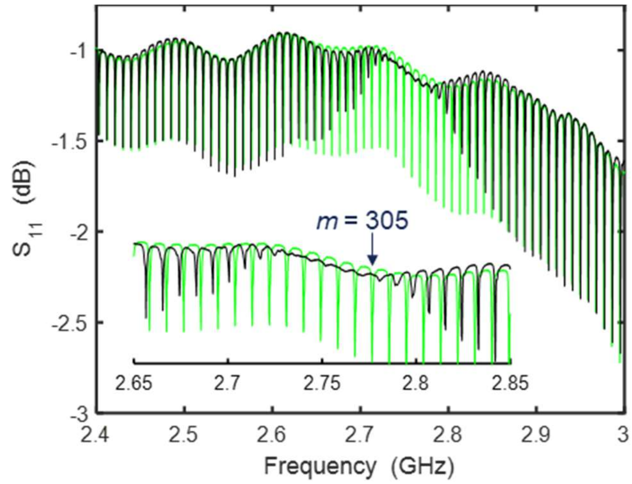

Figure 4. RF reflection spectra (S_{11}) of the wire-bonded and mounted GaN/Cu/YIG ME-HBAR comparing the resonances at zero field (green), and at B_x = 56 mT, B_z = 180 mT (black). Over a range of frequencies, the phonon-magnon coupling causes a frequency shift in the acoustic modes. The inset magnifies the spectral region near m = 305 where phonon-magnon coupling completely attenuates the mechanical mode, effectively switching it off.

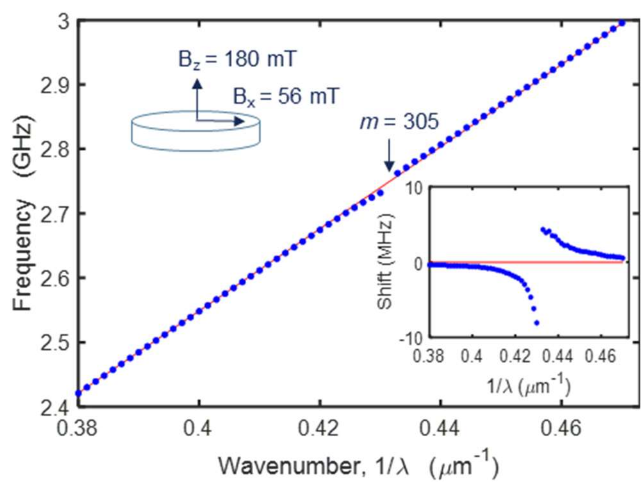

Figure 5. Magnetoelastic dispersion relation of the GaN/Cu/YIG ME-HBAR under the biasing conditions B_x = 56 mT and B_z = 180 mT. The inset shows the magnetoelastic frequency shift from the best-fit linear dispersion.

For a YIG-based ME-HBAR to be used as a tunable magnetoelastic oscillator or a filter, a ~1% tuning range would allow, for example, the active fine-tuning of the center frequency of a narrow-band filter (or an ensemble of periodic narrow-band filter modes that are within the hybridization range), but is insufficient for band switching. The acoustic velocity change due to the ΔE effect is, to first order, proportional to the magnetostriction coefficient λ_s of the magnetic material. YIG has a moderate magnetostriction of λ_s =2.4 ppm. Other ferrites such as Ni-Co-ferrite and Ni-Mn-Co-ferrite have λ_s in excess of 100 ppm [20] and would appear to be promising candidates for MTP resonators with much larger tuning ranges, and could be investigated along similar lines.

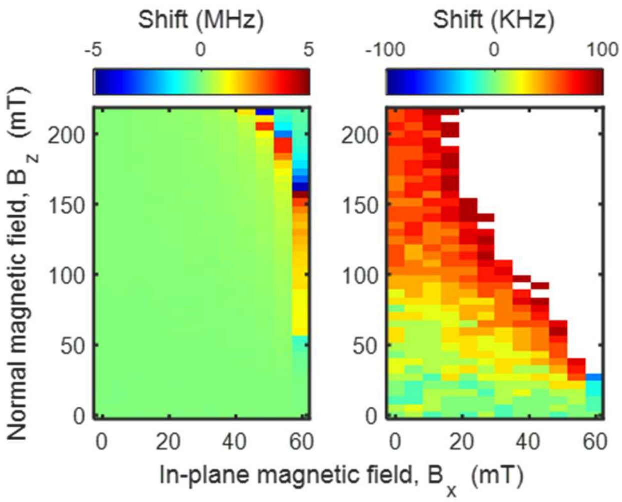

Figure 6. Shift in the frequency of acoustic resonant mode $m = 305$ *(~ 2.75 GHz) as a function of in-plane and normal magnetic field. The shift is relative to zero magnetic field. (a) Large frequency shifts are accompanied by significant damping of the acoustic mode, while (b) frequency tuning with negligible dissipation can be achieved over a smaller range.*

CONCLUSION

We have presented a demonstration of the MTP process that simplifies the often-conflicting demands of integrating incompatible epitaxial thin films and substrates. Unlike wafer-scale piezoelectric film transfer techniques, MTP can integrate various best-in-class RF/acoustic devices, along with electronic or optical components, to an arbitrary target substrate. As an example, we have transferred high quality acoustic transducers made from electronic-grade GaN on to a ferrimagnetic YIG substrate. The resulting ME-HBAR clearly demonstrates phonon-magnon mode coupling. Among other applications, this ME-HBAR can be used as a magnetically tunable RF/acoustic MEMS oscillator or filter. Integrated subsystems consisting of HEMTs, HBARs or other acoustic devices, could be transferred to YIG or other ferroic substrates. Beyond the widely hailed benefits to electronics manufacturing offered by the heterogeneous integration of chiplets, MTP processes can be used to integrate high quality electronic, optical, or acoustic functions on any target substrates appropriate to a particular application.

REFERENCES

[1] B. P. Downey, A. Xie*, et al.*, "Micro-transfer Printing of GaN HEMTs for Heterogeneous Integration and Flexible RF Circuit Design," in *Device Research Conference (DRC)*, 2020, pp. 1-2.

[2] J. Xu, C. Zhong*, et al.*, "Coherent Pulse Echo in Hybrid Magnonics with Multimode Phonons," *Physical Review Applied,* vol. 16, p. 024009, 2021.

[3] N. I. Polzikova, S. G. Alekseev*, et al.*, "Acoustic excitation and electrical detection of spin waves and spin currents in hypersonic bulk waves resonator with YIG/Pt system," *Journal of Magnetism and Magnetic Materials,* vol. 479, pp. 38-42, 2019.

[4] I. Lisenkov, A. Jander, and P. Dhagat, "Magnetoelastic parametric instabilities of localized spin waves induced by traveling elastic waves," *Physical Review B,* vol. 99, p. 184433, 2019.

[5] P. Chowdhury, A. Jander, and P. Dhagat, "Nondegenerate Parametric Pumping of Spin Waves by Acoustic Waves," *IEEE Magnetics Letters,* vol. 8, pp. 1-4, 2017.

[6] P. Chowdhury, P. Dhagat, and A. Jander, "Parametric Amplification of Spin Waves Using Acoustic Waves," *IEEE Transactions on Magnetics,* vol. 51, pp. 1-4, 2015.

[7] J. D. Adam, B. R. McAvoy, and H. L. Salvo, "Magnetically Tunable High Overtone Microwave Resonators," in *40th Annual Symposium on Frequency Control*, 1986, pp. 392-393.

[8] H. L. Salvo, R. A. Moore*, et al.*, "Properties of Tunable Yig Hbars," in *IEEE 1987 Ultrasonics Symposium*, 1987, pp. 337-340.

[9] N. Polzikova, S. Alekseev*, et al.*, "Acoustically driven magnetic excitations in BAW resonators with magnetic layers," in *2013 IEEE International Ultrasonics Symposium (IUS)*, 2013, pp. 216-219.

[10] A. Litvinenko, R. Khymyn*, et al.*, "Tunable Magnetoacoustic Oscillator with Low Phase Noise," *Physical Review Applied,* vol. 15, p. 034057, 2021.

[11] V. J. Gokhale, B. P. Downey*, et al.*, "Epitaxial bulk acoustic wave resonators as highly coherent multi-phonon sources for quantum acoustodynamics," *Nature Communications,* vol. 11, p. 2314, 2020.

[12] V. J. Gokhale, B. P. Downey*, et al.*, "Temperature evolution of frequency and anharmonic phonon loss for multi-mode epitaxial HBARs," *Applied Physics Letters,* vol. 117, p. 124003, 2020.

[13] V. J. Gokhale, B. P. Downey*, et al.*, "Engineering Efficient Acoustic Power Transfer in HBARs and Other Composite Resonators," *Journal of Microelectromechanical Systems,* vol. 29, pp. 1014-1019, 2020.

[14] B. P. Downey, D. S. Katzer*, et al.*, "XeF2 etching of epitaxial Nb2N for lift-off or micromachining of III-N materials and devices," *Journal of Vacuum Science & Technology A: Vacuum, Surfaces, and Films,* vol. 35, p. 05C312, 2017.

[15] *X-Celeprint Ltd*. Available: https://x-celeprint.com/technology

[16] C. Bower, M. Meitl, and R. S. Cok, "Micro-transfer-printed acoustic wave filter device," US Patent 11,139,797, 2021.

[17] H. M. Chou and E. D. Case, "Characterization of some mechanical properties of polycrystalline yttrium iron garnet (YIG) by non-destructive methods," *Journal of Materials Science Letters,* vol. 7, pp. 1217-1220, 1988.

[18] C. Kittel, "Interaction of Spin Waves and Ultrasonic Waves in Ferromagnetic Crystals," *Physical Review,* vol. 110, pp. 836-841, 1958.

[19] F. J. R. Schülein, E. Zallo*, et al.*, "Fourier synthesis of radiofrequency nanomechanical pulses with different shapes," *Nature Nanotechnology,* vol. 10, pp. 512-516, 2015.

[20] A. P. Greifer, "Piezomagnetism of biased ferrites," *Journal of Applied Physics,* vol. 35, pp. 1065-1066, 1964.